



ORIGINAL ARTICLE

Integrating MWCNTs-doped MXene with multi-spiral-channel architecture enables field effect transistor biosensor capable of ultrasensitive determination of methotrexate



Chunwen Lu^a, Ping Xu^b, Dahui Wang^{b,*}, Dong Fu^{b,*}

^a Department of Orthopedics, Changhai Hospital, Second Military Medical University, Shanghai, China

^b Department of Pediatric Orthopedics, Children's Hospital of Fudan University, National Children's Medical Center, Shanghai, China

Received 3 December 2022; accepted 23 April 2023

Available online 28 April 2023

KEYWORDS

MWCNTs-doped MXene;
Multi-spiral;
Field effect transistor;
Biosensor;
Methotrexate

Abstract Previous breakthroughs in biosensor diagnostics stem from engineering and nanocomposites. Accurately detecting low-abundance compounds such as methotrexate in complex biospecimens (e.g. serum) is an important clinical challenge. To address this issue, a MWCNTs-doped MXene-based multi-spiral-channel field-effect transistor (MMSFETs) biosensor was constructed for ultrasensitive quantification of methotrexate. Our integrated biosensor exhibited following merits: a) The synergetic performance of MXene and MWCNTs for enhanced transconductance (0.63 mS) and detection capability (methotrexate, linear range of 0.001–100 μM and LOD down to 0.352 nM); b) Favorable selectivity, stability (one month), reproducibility (RSD = 0.99%, n = 7) for biosensing of methotrexate; c) Acceptable clinical performances on comparisons of MMFETs against commercial Abbott automatic immunoluminescence instrument (ARCHITECT I1000): favorable linearity and correlation coefficient ($Y_{\text{MMSFETs}} = 1.4305 \times X_{\text{targeted concentration}} + 4.3791$ with $R^2 = 0.949$), significant p value ($7.68\text{E-}12 < 0.001$) and diagnosis capability of AUC (0.9907). Those advantages are anticipated to pave an avenue to design of the FETs-based biosensor towards the point-of-care diagnostics applications.

© 2023 The Author(s). Published by Elsevier B.V. on behalf of King Saud University. This is an open access article under the CC BY-NC-ND license (<http://creativecommons.org/licenses/by-nc-nd/4.0/>).

* Corresponding authors.

E-mail addresses: wangdahui@fudan.edu.cn (D. Wang), fudong@fudan.edu.cn (D. Fu).

Peer review under responsibility of King Saud University. Production and hosting by Elsevier.



1. Introduction

The methotrexate, formerly amethopterin, working as an anti-folate chemotherapy and antimetabolite medicine, which has been used to manage various cancer disorders, including but not limited to lymphoma leukemia throphoblastic neoplasm as well as inflammatory agent to cure lupus, rheumatoid (Guo et al., 2021; Le Bras, 2019; Li et al., 2021; Tajik et al., 2022). Nevertheless, disadvantages such as cardiotoxicity, hypoalbuminemia, and myelosuppression have restricted the wide clinical applications under its high doses (El-Said et al., 2019; Jandaghi et al., 2020; Karami et al., 2019; Li et al., 2021; Tajik et al., 2022). Meanwhile, due to its limited presence in complex biosamples, devising an effective approach for the precise and sensitive detection of methotrexate remains a desirable yet formidable task. Accurate determination of methotrexate levels is paramount in furnishing healthcare providers with essential clinical insights.

A variety of techniques including the UV-visible spectrometry (Castro-Puyana et al., 2011), capillary electrophoresis (Cheng et al., 2010), liquid chromatograph mass spectrometer (Wu et al., 2015) and electrochemical biosensor (Castro-Puyana et al., 2011; El-Said et al., 2019; Jandaghi et al., 2020) have been applied for the quantification of methotrexate. In the field of immunosensors, ZnO nanocomposite, multi-walled carbon nanotubes, vanadium oxide have been integrated with glassy carbon electrode or screen-printed electrode for the determination of methotrexate (Chen et al., 2019; Deng et al., 2020; Li et al., 2021; Wang et al., 2014). Nonetheless, there remains scope for enhancement pertaining to its detection capability, encompassing expansion of the detection range and minimization of its lower limit of detection. Nowadays, field effect transistors (FETs) strategy has gained intensive attentions because of its unique merits, including portability & miniaturization, quick response, amplified sensitivity, and high ratio signal ratio (Ji et al., 2018; Kim et al., 2020; Le Gall et al., 2020; Liu et al., 2021; Perera et al., 2013; Xu et al., 2016), resulting in numerous applications in the fields of biosensing (Bischak et al., 2020; Macchia et al., 2020; Sarkar et al., 2014; Sengupta and Hussain, 2021; Seo et al., 2020; Wang et al., 2022). In principle, the intrinsic properties of semiconducting and the architecture of electrodes decide the amplification performance of FETs-based biosensor (Kim et al., 2022; Zamzami et al., 2022b). Therefore, it's desirable to tailor specific semiconducting nanocomposites and property transistor's structure to maximize the quantification capability.

The semiconducting MXene (Eom et al., 2020; Liu et al., 2018; Umrao et al., 2019; Y. Z. Zhang et al., 2020), a typical multiple two-dimensional (2D) nanocomposites with favorable electronic, semiconducting and transport properties. Additionally, in practice, intercalation and delamination structures in MXene provide wide spatial possibility for doping of semiconductor (Bai et al., 2020; Chen et al., 2021; Mojtavavi et al., 2019; Xu et al., 2016; Z. Zhang et al., 2020; Zhu et al., 2020), which would further enhance the quantification performance. The multi-wall carbon nanotubes (MWCNTs) is one of carbon-based nanomaterials with favorable conductivity and biocompatibility (Liang et al., 2020; Türk et al., 2018; Wang et al., 2020), which were also widely used in the field of biosensing. The interdigitated architecture of source-drain electrodes has been intensively reported for enhance the transconductance (G_m) (Paterson et al., 2020; Wu et al., 2019, 2018) of FETs-based biosensor due to the improved efficient semiconducting nanomaterials on the channel. Rational design of the multi-spiral configuration represents a promising approach to amplify the efficacy of field-effect transistor-based biosensors. In light of this, we have devised a biosensor utilizing MWCNTs-doped MXene-based multi-spiral-channel field-effect transistors (MMSFETs) to detect methotrexate with remarkable sensitivity. The novelty of this research lies in the amalgamation of nanocomposite optimization and the intricately tailored design of a multi-spiral configuration, which has yielded outstanding quantification capabilities for the biosensing of methotrexate. Furthermore, we have systematically fine-tuned various pertinent parameters, such as

pH, temperature, and aptamer concentration, to optimize the performance of our biosensor. Furthermore, we undertook a comprehensive assessment of the clinical feasibility of FETs-based biosensors in terms of their future applications. Our biosensor, based on FETs, exhibited a highly favorable linear correlation with targeted methotrexate concentration, along with a marked distinction between biospecimens with low and high concentrations. Additionally, our proposed methodology was able to differentiate between biospecimens with a high concentration of methotrexate and those with a low concentration, with an area under the curve (AUC) value of 0.9907.

2. Materials and methods

2.1. Reagents

The prostate specific antigen (PSA, ab167924), myoglobin (MYO, ab77876), cluster of differentiation 63 (CD63, ab276872), neuron-specific enolase (NSE, ab78797), carbohydrate antigen 19-9 (CA199, ab289665) were bought from Abcam, Inc. The methotrexate (PHR1396), hydrofluoric acid (HF, 184225), glucose (PHR1000), cysteine (C7352) were provided by Sigma Chemical Co. The hydrochloric acid (HCl, 10011028), 6-mercapto-1-hexanol (MCH, XW163378901) were purchased from Sinopharm Chemical Reagent Co. The methotrexate aptamer with sequence of HS-GGAGGCTCTC GGGACGACGGACGCGGGATGTTTGGGGGACCCACG TTTGTCGTCGCCGATGCTGCAATCGTAA for specific binding with methotrexate was provided by Sangon Biotech (Shanghai, China) according to previous literature (He et al., 2021). The MAX phase Ti_3AlC_2 and MWCNTs were provided by Xian Ruixi Biotechnology Co and Chengdu Organic Chemicals Co. Ltd, respectively. The ultrapure deionized (DI) water was processed by a Milli-Q system.

2.2. Synthesis of MXene and doping of MWCNTs/MXene nanocomposites

To synthesize the MXene used in our biosensor, we followed procedures reported in the literature by reported literatures (Hosseini et al., 2020; Yang et al., 2020). Initially, we added 2.0 g Ti_3AlC_2 slowly to a 0.1 M HF solution and stirred the solution continuously for 20 h at 45°C. We then washed the resulting mixture ten times with deionized water until the pH reached 6.6. The black powder was collected via drying in a vacuum oven at 60°C for 12 h to prepare for the doping procedures with MWCNTs and MXene. We prepared various ratios of MWCNTs and MXene (0%, 1.0%, 2.0%, and 3.0% by weight) via strong stirring at 60°C for 2 h. These doped materials were used to construct the multi-spiral-channel field-effect transistor (MMSFETs) biosensor for the ultrasensitive quantification of methotrexate. Overall, the synthesis and preparation procedures were carefully conducted to ensure the high quality and performance of the biosensor.

2.3. Fabrication, functionalizations and reaction of MMSFETs

We fabricated the MMSFETs biosensor via photolithography and thermal evaporation strategies (Fu et al., 2017; Lin et al., 2011; Tang et al., 2011). The photolithography was performed by S1833 (Shipley) with exposure time of 10 s, 365 nm, and 20 mW/cm². The configurations for thermal evaporation were

set as following: 2.6 Pa, 4 nm Cr acting as the adhesive layer and 50 nm Au deposition as the metal interconnection. Finally, the channel was spin-coated with the fixed ratio MWCNTs/MXene mixture following by 1 h bakeout under 60 °C. For the functionalization of gate electrode, the MMSFETs was cleaned with plasma for 5 min and incubated in the 20 μ M aptamer for 4 h. Then, the MMSFETs was blocked by 20 μ M MCH for 10 h to avoid nonspecific adsorption (Anjum et al., 2019). Finally, the functionalized MMSFETs biosensors were kept in 4 °C refrigerator for further usage. For the determination of methotrexate, the MMSFETs

biosensors were incubation with a series of methotrexate solutions or clinical biosamples with optimal parameters including the temperature (37 °C), incubation time (40 mins), and pH (7.0) (See detailed information in 3.3) for the evaluation of the performance.

2.4. Characterizations of MMSFETs

The MWCNTs/MXene nanocomposites were characterized by scanning electron microscope (SEM) via EM-30AX. The AFM

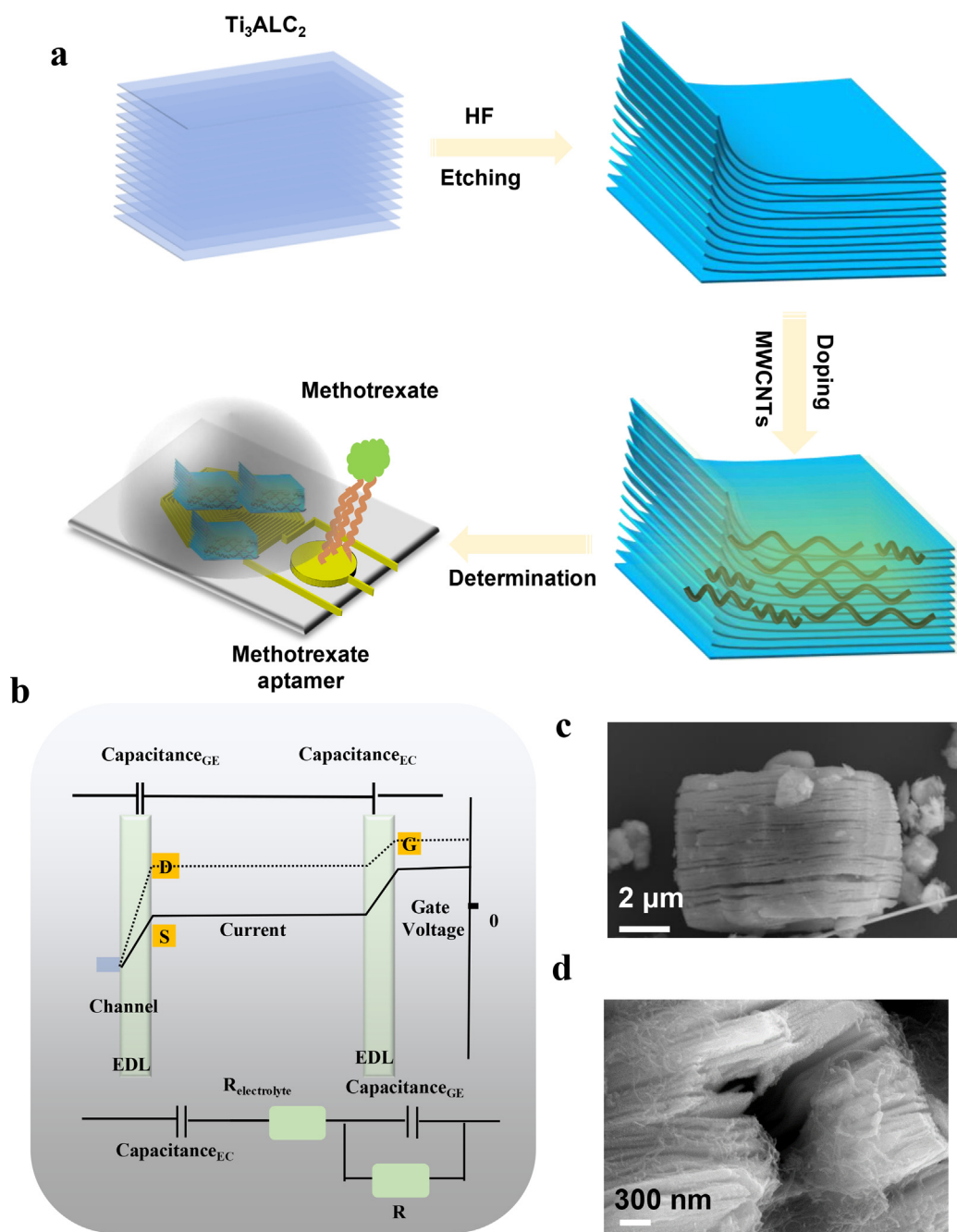


Fig. 1 A) illustrative scheme of fabrication of hybrid MMSFETs for ultrasensitive determination of methotrexate. b) The mechanism of field effect transistor and corresponding electrical double layers (EDLs). SEM photography of c) pristine MXene and d) MWCNTs-doped MXene.

analysis of bare gate, gate/aptamer, gate/aptamer/MCH and gate/aptamer/MCH/methotrexate were performed by AFM Dimension FastScan (Bruker). The transfer characteristics of MMSFETs were measured by Keithley sourcemeter 2400. Typically, the electrodes including the gate, source and drain of MMSFETs were immersed in PBS ionic liquid electrolyte, and the sourcemeter 2400 would record the amperometric signal of channel. Because the binding between the methotrexate and the aptamer in MMSFETs would lead the increase of resistance for gate electrode, and the biosensor would amplify the small signal into favorable readout, resulting in the correction relationship between the amperometric signal and the targeted concentration of methotrexate.

2.5. Harvesting of biosamples

The institutional ethics committee of the Children's Hospital of Fudan University proved all clinical research and protocols in this project. For the protocols of biospecimens harvesting, five milliliter of biospecimens were collected under centrifugation with configurations of $1500 \times g$ and 8 min. The obtained biospecimens were stored for further quantification (-20°C).

The AUC, *t*-test and calibration curve were analyzed by GraphPad Prism 9.

3. Results

3.1. Illustrative mechanism and characterization of MMSFETs

To attain highly sensitive and precise quantification of methotrexate, we employed a customized design approach to develop a hybrid biosensor utilizing MWCNTs-doped MXene-based multi-spiral-channel field-effect transistors (Fig. 1a). The FETs-based biosensor has the ability to amplify otherwise imperceptible signals into discernable readouts via the utilization of electrical double layers (EDLs, Fig. 1b). As the semiconductor for our biosensor, we opted for 2-D semiconducting MXene nanocomposites, which exhibited clear intercalation and delamination structures (Fig. 1c). We also performed elemental mapping to validate the synthesis of MXene (Fig. S1-2 and Supporting Table S1), with conclusive evidence of the existence of Ti, C, N, and O. Additionally, we verified the doping of MXene with MWCNTs to enable subsequent optimization of our biosensors (Fig. 1d).

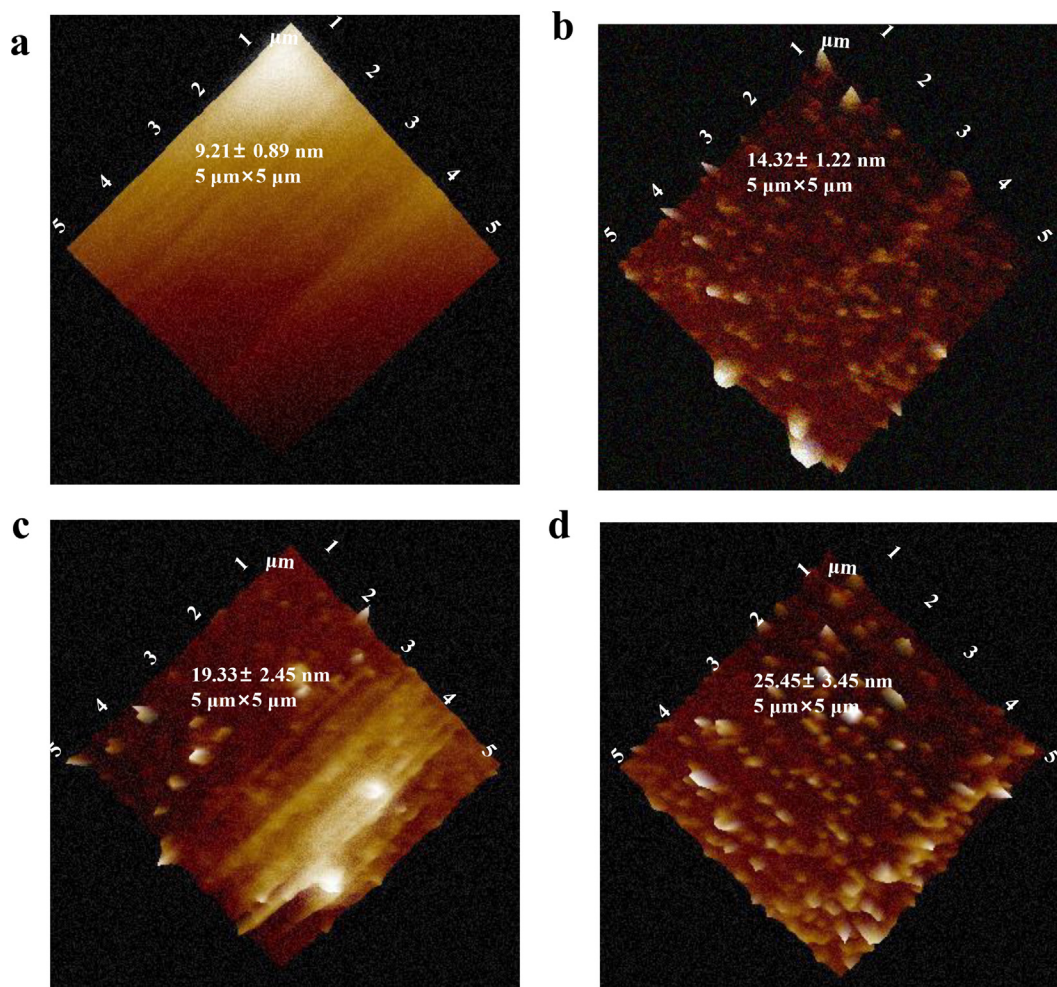


Fig. 2 Validations of functionalization procedures for MMSFETs. AFM analysis of a) original gate, b) gate/aptamer, c) gate/aptamer/MCH, d) gate/aptamer/MCH/methotrexate, respectively.

3.2. Validation of modification processes

To achieve highly specific quantification of methotrexate, we selected a customized aptamer with the sequence HS-GAGGCTCTCGGGACGACGACGCGGGATGTTTGGGGGACCCACGTTTGTCTGCCGATGCTGCAATCGTAA, which exhibited specific binding affinity towards methotrexate. To validate the successful functionalization of aptamer and efficient blocking, we employed atomic force microscopy (AFM) and utilized root mean square (RMS) roughness (Jia et al., 2019; Lee et al., 2018; Seo et al., 2020; Zhang et al., 2012) as the index for evaluating the modification procedures (Fig. 2-a-d). The pristine gold electrode exhibited the lowest RMS value of 9.21 ± 0.89 nm. When the gate electrode was functionalized with 20 μ M aptamer, the RMS value for gate aptamer increased to 14.32 ± 1.22 nm. Following the blocking of MCH, the RMS value for the gate/aptamer/MCH electrode further increased. Finally, the highest RMS value was observed for the gate/aptamer/MCH electrode due to the specific binding between the aptamer and methotrexate.

3.3. Detection performance optimization of MMSFETs

To optimize the detection performance MMSFETs, we systematically tailored the semiconducting and the architecture of transistor. The signal response of MMSFETs was enhanced

as the increase of aptamer concentration at relatively high value with 10.9 ± 0.87 μ A (Fig. 3a). Meanwhile, the Δ drain-source demonstrated a trend of first rising and then falling with maximum of 10.4 ± 0.41 μ A (Fig. 3b). For the optimization of specific binding between the aptamer and the methotrexate, the optimal parameter for binding temperature and binding time were selected at 37°C and 40 min, respectively (Fig. 3c-d). Optimizing aptamer concentration and incubation time is crucial for achieving sufficient binding between methotrexate and aptamer. In terms of pH and temperature, there is a general rising trend followed by a decline, as exceedingly high pH and temperature can adversely impact the biochemical interaction between methotrexate and aptamer. With the aforementioned optimizations, the optimal configurations for designing and functionalizing the MMSFETs biosensor can be ensured.

The optimizations of semiconducting nanocomposites and the tailored channel architecture are critical factors for maximization of detection capability (Zamzami et al., 2022a). We tailored the doping of MWCNTs into MXene including the ratio of 0.0%, 1.0 %, 2.0% and 3.0% in Fig. 4a-d. We analyzed the transfer characteristics and corresponding transconductance, because the G_m represented the detection sensitivity. The detection capability of MMSFETs improved as the increase of MWCNTs doping ratio from 0% to 2.0% with a maximum of 0.63 mS. Subsequently, although the

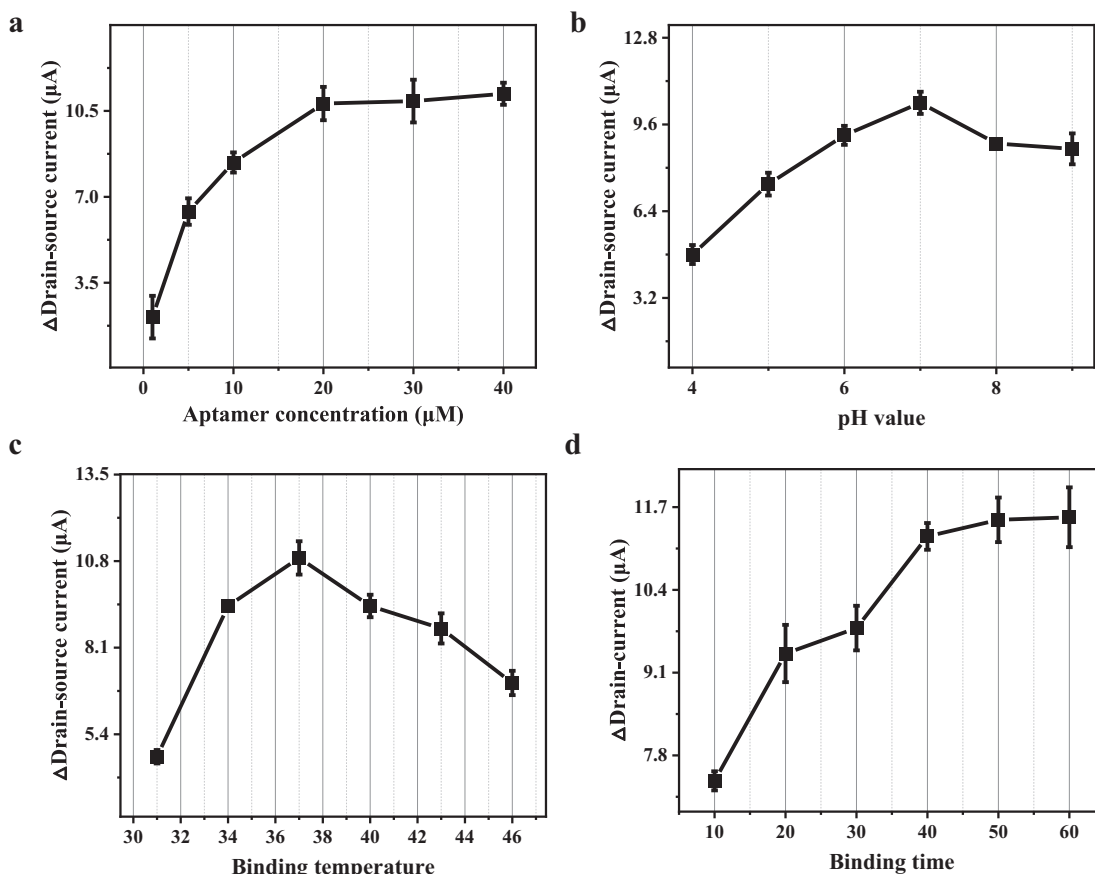


Fig. 3 Optimal configurations for MMSFETs biosensor. Optimizations of a) aptamer concentration, b) pH value, c) binding temperature and d) binding time for maximum of detection performance. Error bars in (a-d) were calculated by the standard deviation (SD) of three replicate measurements (n = 3).

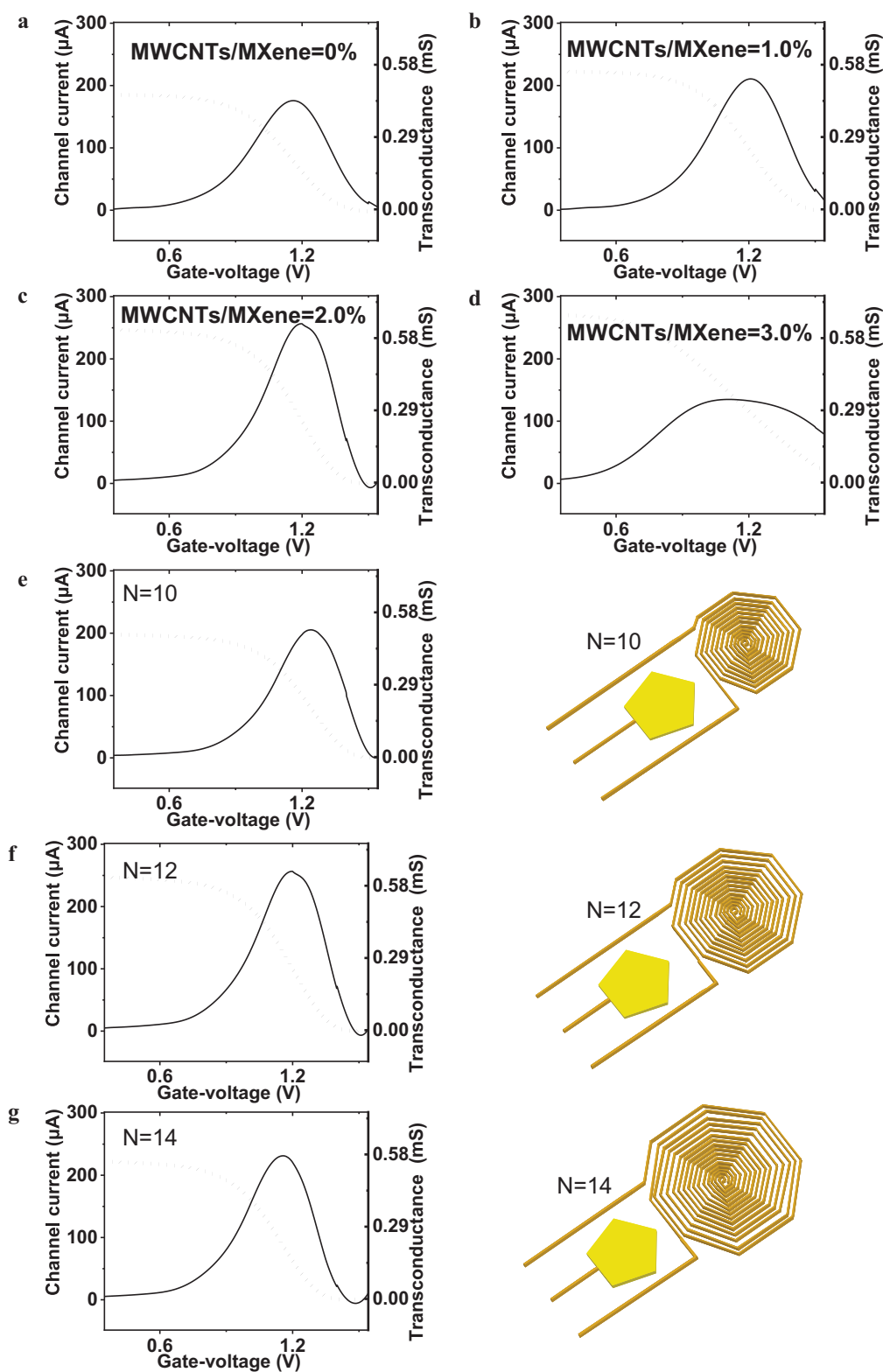


Fig. 4 Optimizations of MWCNTs ratio and the electrode architectures. Transfer characteristics and corresponding transconductance (G_m) analysis of MMSFETs biosensor with MXene/MWCNTs as the semiconducting when the doping ratio at a) 0%, b) 1.0%, c) 2.0, d) 3.0. Transfer characteristics and G_m analysis for multi-spiral-channel MMSFETs biosensor with e) $N = 10$, f) $N = 12$, g) $N = 14$.

3.0% MWCNTs doping ratio enhanced the original drain-source amperometric current, the semiconducting property diminished, resulting in declined G_m (Fig. 4d). We hypothe-

sized that with the increase of MWCNTs concentration, the gain of G_m has a trend of rising first and then falling, which is due to its internal dynamic balance. Our field effect transis-

tor biosensor would amplify the negligible signal into notable readout via the electrical double layers (EDLs, Fig. 1b). The channel architecture especially effective area is the key configuration for the optimization of MMSFETs. Herein, we performed transfer characteristics and Gm analysis for multi-spiral-channel MMSFETs biosensor with N = 10, N = 12, N = 14, and the N = 12 demonstrated the optimum performance (Fig. 4e-g). Abovementioned optimizations on nanoma-

terials and the electrode architecture established a robust groundwork for subsequent methotrexate quantification.

3.4. Selectivity, reproducibility, stability and quantification capability

To verify the usability of MMSFETs, we performed the selectivity evaluation via comparing the response signal of

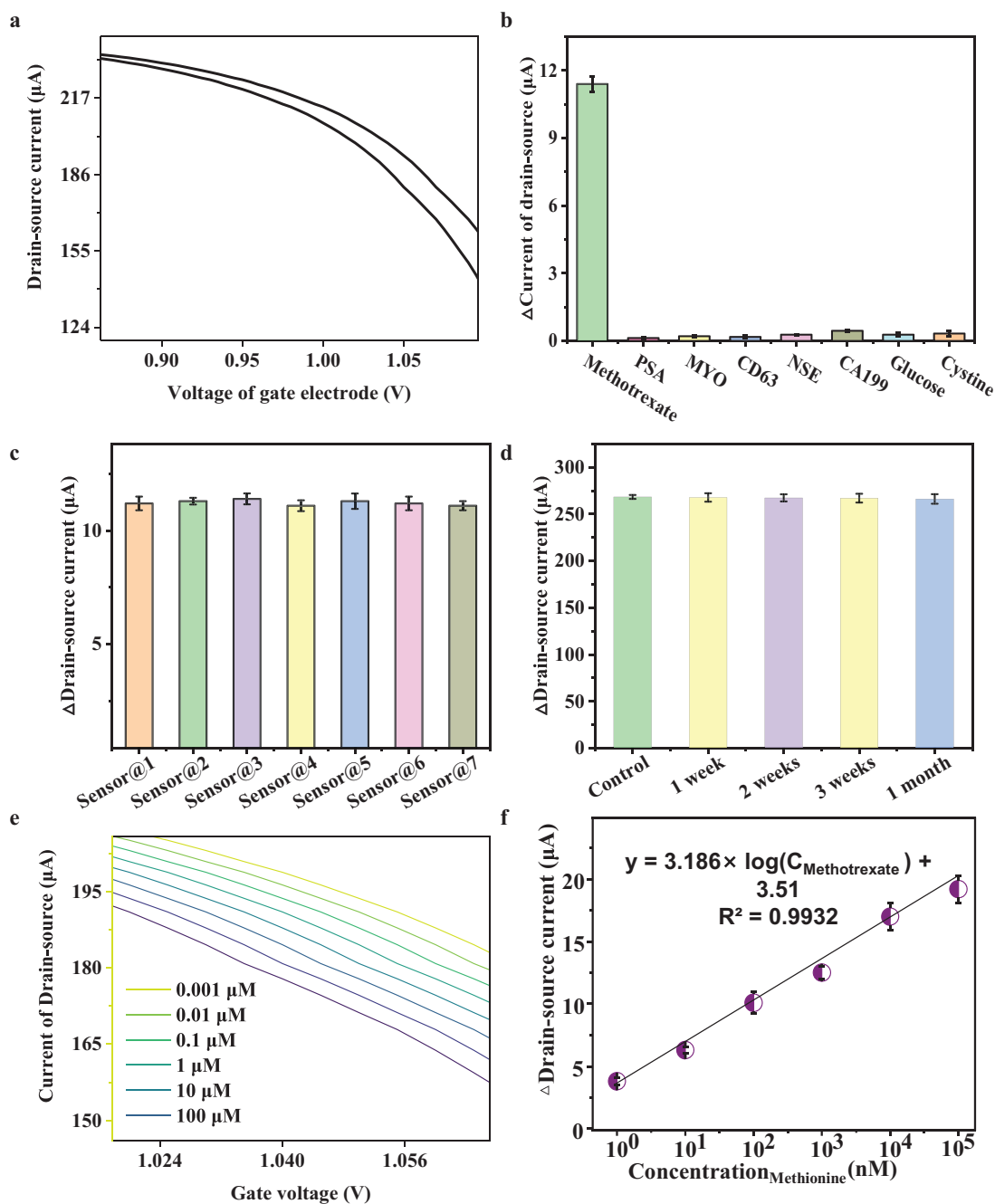


Fig. 5 A) amperometric responses of mmsfets biosensor for detection of methotrexate, b) selectivity of mmsfets for biosensing of methotrexate against other interferences including psa, myo, cd63, nse, ca199, glucose and cystine. c) reproducibility of seven mmsfets biosensor. d) stability of mmsfets biosensor. e) a variety of methotrexate ranging from 0.001 to 100 μM was detected by MMSFETs and f) corresponding calibration curve. Error bars in (b-d, f) were calculated by the standard deviation (SD) of three replicate measurements ($n = 3$).

methotrexate against other interferences including CD63, PSA, MYO, NSE, CA199, glucose and cystine (Fig. 5a-b). The favorable response signal of MMSFETs biosensing of 100 nM methotrexate were observed with $11.4 \pm 0.34 \mu\text{A}$, while negligible response signals of PSA ($0.13 \pm 0.04 \mu\text{A}$), YO ($0.21 \pm 0.03 \mu\text{A}$), CD63 ($0.18 \pm 0.05 \mu\text{A}$), NSE ($0.28 \pm 0.02 \mu\text{A}$), CA199 ($0.45 \pm 0.04 \mu\text{A}$), glucose ($0.28 \pm 0.08 \mu\text{A}$) and cysteine ($0.33 \pm 0.12 \mu\text{A}$) were displayed in Fig. 5b, which evidenced acceptable selectivity of MMSFETs for quantification of methotrexate. For the evaluation of stability, we recorded the amperometric response of MMSFETs for quantification of methotrexate, resulting in a relative standard derivation (RSD) of 0.99%, which confirmed the favorable stability of MMSFETs biosensor (Fig. 5c). Moreover, we also monitored the stability of MMSFETs for further applications. Specifically, we monitored the amperometric signals of MMSFETs over 1 month, with a maximum of signal decline by 0.82%, which proved the favorable stability of MMSFETs (Fig. 5d). Finally, we performed quantification for a series of concentrations ranging from 0.001 to 100 μM via the transfer characteristics (Fig. 5e), the calibration curve was plotted with favorable linear correlation $y = 3.186 \times \log C_{\text{Methotrexate}} + 3.51$ with $R^2 = 0.9932$ (Fig. 5f). Meaningful, we calculated the limit of detection low to 0.352 nM via the signal noise ratio at 3.0 according to previous literatures (Bischak et al., 2020;

Zhang et al., 2019a; Zhao et al., 2018). Meanwhile, we have compared our results with those of other state-of-the-art biosensors listed in Table S2. The MMSFETs biosensor exhibited an enhanced determination capability for biosensing methotrexate, with improvements observed in the detection range and limit of detection (Table S2).

3.5. Clinical performances of MMSFETs

To establish a practical platform for clinical applications, we collected 65 biospecimens, consisting of 23 samples with elevated methotrexate concentration and 42 samples with low concentration ranging from 0 to 10 μM , for comprehensive assessment (Fig. 6a, Table S3). Our MMSFETs biosensors were employed to detect methotrexate in all 65 biospecimens and subsequently compared with the targeted concentrations. The correlation between the measured concentration of methotrexate (by MMSFETs biosensors) and the intended concentration was analyzed with high accuracy, yielding a linear correction model of $Y_{\text{MMSFETs}} = 1.4305 \times X_{\text{targeted concentration}} + 4.3791$, with an impressive R^2 value of 0.949 (Fig. 6b). Furthermore, our *t*-test analysis demonstrated a significant difference between the low and high concentrations of methotrexate measured by MMSFETs for all biospecimens ($p = 7.68\text{E-}12 < 0.001$,

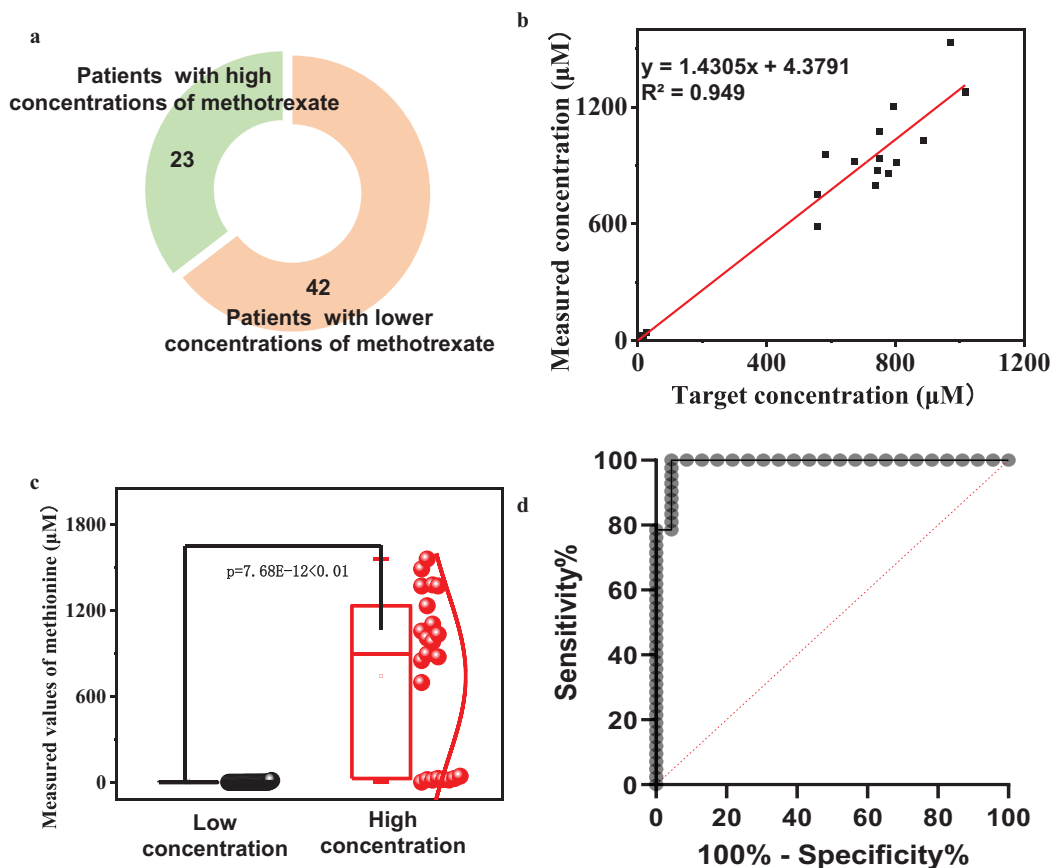


Fig. 6 Clinic deployment of MMSFETs. a) Clinical information of 65 biospecimens including 23 patients with high concentration of methotrexate and 42 patients ($> 10 \mu\text{M}$) with low concentration (0–10 μM). b) The linear correction between targeted concentration and the measured concentration (by MMSFETs biosensors) for total 65 biospecimens. c) The *t*-test analysis demonstrated obvious significance between the low and high concentration measured by MMSFETs for all biospecimens. d) AUC analysis with value of 0.9907 (Sensitivity of 100% and specificity of 95.65%) for discrimination of biosamples with high concentration from low concentration via MMSFETs.

Fig. 6c). The t-tests for independent low-concentrations and high-concentrations were analyzed individually, resulting in R^2 values of 0.9923 and 0.9902, respectively (Fig. S3-4). Lastly, we performed an area under curve (AUC) analysis, which yielded a value of 0.9907 (with sensitivity of 100% and specificity of 95.65%) for discriminating between high and low concentrations of methotrexate via MMSFETs (Fig. 6d). The above-mentioned outcomes conclusively demonstrate the clinical usability of MMSFETs in detecting real biospecimens.

4. Conclusions

In summary, our study presents a novel hybrid MWCNTs-doped MXene-based multi-spiral-channel field-effect transistor (MMSFETs) biosensor for highly sensitive detection of methotrexate. The integration of MWCNTs-doped MXene and multi-spiral-channel architecture into the field-effect transistor provided exceptional sensitivity for methotrexate detection within the range of 0.001–100 μM with an unprecedentedly low LOD of 0.352 nM, surpassing the performance of previously reported biosensors. We optimized the parameters such as pH and temperature to ensure excellent selectivity, reproducibility (RSD = 0.99%, $n = 7$) and stability (over one month). Our MMSFETs biosensor demonstrated excellent diagnostic performance in clinical biospecimens, as evidenced by the high linear correlation ($Y_{\text{MMSFETs}} = 1.4305 \times X_{\text{targeted concentration}} + 4.3791$ with $R^2 = 0.949$), low p value ($7.68\text{E-}12 < 0.001$), and high AUC value (0.9907). Overall, considering the above-mentioned merits, we anticipate that MMSFETs biosensor paves a practical platform for field effect transistor biosensor in the biochemical quantification in clinics.

5. Informed consent statement

Informed consent was obtained from all subjects involved in the investigation.

Funding

This research was funded by Shanghai Sailing Program (21YF403500).

Declaration of Competing Interest

The authors declare that they have no known competing financial interests or personal relationships that could have appeared to influence the work reported in this paper.

Appendix A. Supplementary data

The following are available online at <https://www.mdpi.com/xxx/s1>, Fig. S1: EDS analysis of MXene, Fig. S2: The elemental analysis of MXene, Fig. S3: The linear correlation of methotrexate's targeted concentration and measured concentration when methotrexate with the high concentration, Fig. S4: The linear correlation of methotrexate's targeted concentration and measured concentration with methotrexate's concentrations rana between the 0–10 μM . Table S1: The elemental ratio of MXene. Table S2: The comparisons of biosensors for quantification of methotrexate. Table S3. Clinical information of 65 biospecimens.

Supplementary data to this article can be found online at <https://doi.org/10.1016/j.arabjc.2023.104943>.

References

- Anjum, M., Madsen, J.S., Nesme, J., Jana, B., Wiese, M., Jasinskyte, D., Nielsen, D.S., Sørensen, S.J., Dalsgaard, A., Moodley, A., Bortolaia, V., Guardabassi, L., 2019. Fate of CMY-2-encoding plasmids introduced into the human fecal microbiota by exogenous *Escherichia coli*. *Antimicrob. Agents Chemother.* 63, 25. <https://doi.org/10.1128/AAC.02528-18>.
- Bai, S., Guo, X., Chen, T., Zhang, Y., Zhang, X., Yang, H., Zhao, X., 2020. Solution processed fabrication of silver nanowire-MXene@-PEDOT: PSS flexible transparent electrodes for flexible organic light-emitting diodes. *Compos. Part A Appl. Sci. Manuf.* 139, <https://doi.org/10.1016/j.compositesa.2020.106088> 106088.
- Bischak, C.G., Flagg, L.Q., Ginger, D.S., 2020. Ion Exchange Gels Allow Organic Electrochemical Transistor Operation with Hydrophobic Polymers in Aqueous Solution. *Adv. Mater.* 32, 1–7. <https://doi.org/10.1002/adma.202002610>.
- Castro-Puyana, M., Lammers, I., Buijs, J., Gooijer, C., Ariese, F., 2011. Quenched phosphorescence as alternative detection mode in the chiral separation of methotrexate by electrokinetic chromatography. *Anal. Bioanal. Chem.* 400, 2913–2919. <https://doi.org/10.1007/s00216-011-4991-6>.
- Chen, J., Li, Y., Jiang, Y., Mao, L., Lai, M., Jiang, L., Liu, H., Nie, Z., 2021. TiO₂/MXene-Assisted LDI-MS for Urine Metabolic Profiling in Urinary Disease. *Adv. Funct. Mater.* 31. <https://doi.org/10.1002/adfm.202106743>.
- Cheng, H.L., Chiou, S.S., Liao, Y.M., Lu, C.Y., Chen, Y.L., Wu, S. M., 2010. Analysis of methotrexate and its eight metabolites in cerebrospinal fluid by solid-phase extraction and triple-stacking capillary electrophoresis. *Anal. Bioanal. Chem.* 398, 2183–2190. <https://doi.org/10.1007/s00216-010-4152-3>.
- El-Said, W.A., Abdel-Rahman, M.A., Sayed, E.M., Abdel-Wahab, A. M.A., 2019. Electrochemical Monitoring of Methotrexate Anticancer Drug in Human Blood Serum by Using in situ Solvothermal Synthesized Fe₃O₄/ITO Electrode. *Electroanalysis* 31, 829–837. <https://doi.org/10.1002/elan.201800798>.
- Eom, W., Shin, H., Ambade, R.B., Lee, S.H., Lee, K.H., Kang, D.J., Han, T.H., 2020. Large-scale wet-spinning of highly electroconductive MXene fibers. *Nat. Commun.* 11, 2. <https://doi.org/10.1038/s41467-020-16671-1>.
- Fu, Y., Wang, N., Yang, A., Law, H.K. wai, Li, L., Yan, F., 2017. Highly Sensitive Detection of Protein Biomarkers with Organic Electrochemical Transistors. *Adv. Mater.* 29, 1–7. <https://doi.org/10.1002/adma.201703787>.
- Guo, Z., Smutok, O., Johnston, W.A., Walden, P., Ungerer, J.P.J., Peat, T.S., Newman, J., Parker, J., Nebl, T., Hepburn, C., Melman, A., Suderman, R.J., Katz, E., Alexandrov, K., 2021. Design of a methotrexate-controlled chemical dimerization system and its use in bio-electronic devices. *Nat. Commun.* 12. <https://doi.org/10.1038/s41467-021-27184-w>.
- He, J., Wang, J., Zhang, M., Shi, G., 2021. Selection of a Structure-Switching Aptamer for the Specific Methotrexate Detection. *ACS Sensors.* <https://doi.org/10.1021/acssensors.1c00749>.
- Hosseini, E., Arjmand, M., Sundararaj, U., Karan, K., 2020. Filler-Free Conducting Polymers as a New Class of Transparent Electromagnetic Interference Shields. *ACS Appl. Mater. Interfaces* 12, 28596–28606. <https://doi.org/10.1021/acsaami.0c03544>.
- Jandaghi, N., Jahani, S., Foroughi, M.M., Kazemipour, M., Ansari, M., 2020. Cerium-doped flower-shaped ZnO nano-crystallites as a sensing component for simultaneous electrochemical determination of epirubicin and methotrexate. *Microchim. Acta* 187. <https://doi.org/10.1007/s00604-019-4016-2>.
- Ji, X., Zhou, P., Zhong, L., Xu, A., Tsang, A.C.O., Chan, P.K.L., 2018. Smart Surgical Catheter for C-Reactive Protein Sensing Based on an Imperceptible Organic Transistor. *Adv. Sci.* 5. <https://doi.org/10.1002/advs.201701053>.

- Jia, X., Hu, M., Soundarapandian, K., Yu, X., Liu, Z., Chen, Z., Narita, A., Müllen, K., Koppens, F.H.L., Jiang, J., Tielrooij, K.J., Bonn, M., Wang, H.I., 2019. Kinetic Ionic Permeation and Interfacial Doping of Supported Graphene. *Nano Lett.* 19, 9029–9036. <https://doi.org/10.1021/acs.nanolett.9b04053>.
- Karami, F., Ranjbar, S., Ghasemi, Y., Negahdaripour, M., 2019. Analytical methodologies for determination of methotrexate and its metabolites in pharmaceutical, biological and environmental samples. *J. Pharm. Anal.* 9, 373–391. <https://doi.org/10.1016/j.jpfa.2019.06.001>.
- Kim, J., Jeong, S., Sarawut, S., Kim, H., Son, S.U., Lee, S., Rabbani, G., Kwon, H., Lim, E.K., Ahn, S.N., Park, S.H.K., 2022. An immunosensor based on a high performance dual-gate oxide semiconductor thin-film transistor for rapid detection of SARS-CoV-2. *Lab Chip* 22, 899–907. <https://doi.org/10.1039/d1lc01116b>.
- Kim, S., Myeong, G., Shin, W., Lim, H., Kim, B., Jin, T., Chang, S., Watanabe, K., Taniguchi, T., Cho, S., 2020. Thickness-controlled black phosphorus tunnel field-effect transistor for low-power switches. *Nat. Nanotechnol.* 15, 203–206. <https://doi.org/10.1038/s41565-019-0623-7>.
- Le Bras, A., 2019. No benefit of methotrexate on the risk of cardiovascular events. *Nat. Rev. Cardiol.* 16, 2–3. <https://doi.org/10.1038/s41569-018-0133-6>.
- Le Gall, J., Mouillard, F., Le, T.N., Vu, T.T., Mattana, G., Brayner, R., Zrig, S., Noël, V., Piro, B., 2020. Monitoring photosynthetic microorganism activity with an electrolyte-gated organic field effect transistor. *Biosens. Bioelectron.* 157, 2–4. <https://doi.org/10.1016/j.bios.2020.112166>.
- Lee, W., Kobayashi, S., Nagase, M., Jimbo, Y., Saito, I., Inoue, Y., Yambe, T., Sekino, M., Malliaras, G.G., Yokota, T., Tanaka, M., Someya, T., 2018. Nonthrombogenic, stretchable, active multielectrode array for electroanatomical mapping. *Sci. Adv.* 4, 1–8. <https://doi.org/10.1126/sciadv.aau2426>.
- Li, J., Chen, D., Zhang, T., Chen, G., 2021. Highly sensitive electrochemical determination of methotrexate based on a N-doped hollow nanocarbon sphere modified electrode. *Anal. Methods* 13, 117–123. <https://doi.org/10.1039/d0ay01996h>.
- Liang, Y., Xiao, M., Wu, D., Lin, Y., Liu, L., He, J., Zhang, G., Peng, L.M., Zhang, Z., 2020. Wafer-Scale Uniform Carbon Nanotube Transistors for Ultrasensitive and Label-Free Detection of Disease Biomarkers. *ACS Nano* 14, 8866–8874. <https://doi.org/10.1021/acsnano.0c03523>.
- Lin, P., Luo, X., Hsing, I.M., Yan, F., 2011. Organic electrochemical transistors integrated in flexible microfluidic systems and used for label-free DNA sensing. *Adv. Mater.* 23, 4035–4040. <https://doi.org/10.1002/adma.201102017>.
- Liu, R., Miao, M., Li, Y., Zhang, J., Cao, S., Feng, X., 2018. Ultrathin Biomimetic Polymeric Ti(3)C(2)T (x) MXene Composite Films for Electromagnetic Interference Shielding. *ACS Appl. Mater. Interfaces* 10, 44787–44795. <https://doi.org/10.1021/acsnano.8b18347>.
- Liu, N., Xiang, X., Fu, L., Cao, Q., Huang, R., Liu, H., Han, G., Wu, L., 2021. Regenerative field effect transistor biosensor for in vivo monitoring of dopamine in fish brains. *Biosens. Bioelectron.* 188. <https://doi.org/10.1016/j.bios.2021.113340>.
- Macchia, E., Manoli, K., Di Franco, C., Picca, R.A., Österbacka, R., Palazzo, G., Torricelli, F., Scamarcio, G., Torsi, L., 2020. Organic Field-Effect Transistor Platform for Label-Free, Single-Molecule Detection of Genomic Biomarkers. *ACS Sensors* 5, 1822–1830. <https://doi.org/10.1021/acssensors.0c00694>.
- Mojtabavi, M., Vahidmohammadi, A., Liang, W., Beidaghi, M., Wanunu, M., 2019. Single-Molecule Sensing Using Nanopores in Two-Dimensional Transition Metal Carbide (MXene) Membranes. *ACS Nano* 13, 3042–3053. <https://doi.org/10.1021/acsnano.8b08017>.
- Paterson, A.F., Savva, A., Wustoni, S., Tsetseris, L., Paulsen, B.D., Faber, H., Emwas, A.H., Chen, X., Nikiforidis, G., Hidalgo, T.C., Moser, M., Maria, I.P., Rivnay, J., McCulloch, I., Anthopoulos, T. D., Inal, S., 2020. Water stable molecular n-doping produces organic electrochemical transistors with high transconductance and record stability. *Nat. Commun.* 11, 1–11. <https://doi.org/10.1038/s41467-020-16648-0>.
- Perera, M.M., Lin, M.W., Chuang, H.J., Chamlagain, B.P., Wang, C., Tan, X., Cheng, M.M.C., Tománek, D., Zhou, Z., 2013. Improved carrier mobility in few-layer MoS₂ field-effect transistors with ionic-liquid gating. *ACS Nano* 7, 4449–4458. <https://doi.org/10.1021/nn401053g>.
- Sarkar, D., Liu, W., Xie, X., Anselmo, A.C., Mitragotri, S., Banerjee, K., 2014. MoS₂ field-effect transistor for next-generation label-free biosensors. *ACS Nano* 8, 3992–4003. <https://doi.org/10.1021/nn5009148>.
- Sengupta, J., Hussain, C.M., 2021. Graphene-based field-effect transistor biosensors for the rapid detection and analysis of viruses: A perspective in view of COVID-19. *Carbon Trends* 2. <https://doi.org/10.1016/j.cartre.2020.100011>.
- Seo, G., Lee, G., Kim, M.J., Baek, S.H., Choi, M., Ku, K.B., Lee, C. S., Jun, S., Park, D., Kim, H.G., Kim, S.J., Lee, J.O., Kim, B.T., Park, E.C., Kim, S.I., 2020. Rapid Detection of COVID-19 Causative Virus (SARS-CoV-2) in Human Nasopharyngeal Swab Specimens Using Field-Effect Transistor-Based Biosensor. *ACS Nano* 14, 5135–5142. <https://doi.org/10.1021/acsnano.0c02823>.
- Tajik, S., Beitollahi, H., Shahsavari, S., Nejad, F.G., 2022. Simultaneous and selective electrochemical sensing of methotrexate and folic acid in biological fluids and pharmaceutical samples using Fe₃O₄/ppy/Pd nanocomposite modified screen printed graphite electrode. *Chemosphere* 291. <https://doi.org/10.1016/j.chemosphere.2021.132736>.
- Tang, H., Lin, P., Chan, H.L.W., Yan, F., 2011. Highly sensitive dopamine biosensors based on organic electrochemical transistors. *Biosens. Bioelectron.* 26, 4559–4563. <https://doi.org/10.1016/j.bios.2011.05.025>.
- Türk, S., Altınsoy, I., Çelebi Efe, G., Ipek, M., Özacar, M., Bindal, C., 2018. 3D porous collagen/functionalized multiwalled carbon nanotube/chitosan/hydroxyapatite composite scaffolds for bone tissue engineering. *Mater. Sci. Eng. C Mater. Biol. Appl.* 92, 757–768. <https://doi.org/10.1016/j.msec.2018.07.020>.
- Umrao, S., Tabassian, R., Kim, J., Nguyen, V.H., Zhou, Q., Nam, S., Oh, I.-K., 2019. MXene artificial muscles based on ionically cross-linked Ti(3)C(2)T (x) electrode for kinetic soft robotics. *Sci. Robot.* 4. <https://doi.org/10.1126/scirobotics.aaw7797>.
- Wang, L., Xie, S., Wang, Z., Liu, F., Yang, Y., Tang, C., Wu, X., Liu, P., Li, Y., Saiyin, H., Zheng, S., Sun, X., Xu, F., Yu, H., Peng, H., 2020. Functionalized helical fibre bundles of carbon nanotubes as electrochemical sensors for long-term in vivo monitoring of multiple disease biomarkers. *Nat. Biomed. Eng.* 4, 159–171. <https://doi.org/10.1038/s41551-019-0462-8>.
- Wang, B., Zhao, C., Wang, Z., Yang, K.A., Cheng, X., Liu, W., Yu, W., Lin, S., Zhao, Y., Cheung, K.M., Lin, H., Hojaiji, H., Weiss, P. S., Stojanović, M.N., Tomiyama, A.J., Andrews, A.M., Emaminejad, S., 2022. Wearable aptamer-field-effect transistor sensing system for noninvasive cortisol monitoring. *Sci. Adv.* 8, 1–16. <https://doi.org/10.1126/sciadv.abk0967>.
- Wu, X., Surendran, A., Ko, J., Filonik, O., Herzig, E.M., Müller-Buschbaum, P., Leong, W.L., Kim, S.M., Kim, C.H., Kim, Y., Kim, N., Lee, W.J., Lee, E.H., Kim, D., Park, S., Lee, K., Rivnay, J., Yoon, M.H., 2018. Ionic-Liquid Doping Enables High Transconductance, Fast Response Time, and High Ion Sensitivity in Organic Electrochemical Transistors. *Nat. Commun.* 9, 201805544.
- Wu, X., Surendran, A., Ko, J., Filonik, O., Herzig, E.M., Müller-Buschbaum, P., Leong, W.L., 2019. Ionic-Liquid Doping Enables High Transconductance, Fast Response Time, and High Ion Sensitivity in Organic Electrochemical Transistors. *Adv. Mater.* 31, 1–9. <https://doi.org/10.1002/adma.201805544>.
- Wu, D., Wang, Y., Sun, Y., Ouyang, N., Qian, J., 2015. A simple, rapid and reliable liquid chromatography–mass spectrometry method for determination of methotrexate in human plasma and

- its application to therapeutic drug monitoring. *Biomed. Chromatogr.* 29, 1197–1202. <https://doi.org/10.1002/bmc.3408>.
- Xu, B., Zhu, M., Zhang, W., Zhen, X., Pei, Z., Xue, Q., Zhi, C., Shi, P., 2016. Ultrathin MXene-Micropattern-Based Field-Effect Transistor for Probing Neural Activity. *Adv. Mater.* 28, 3333–3339. <https://doi.org/10.1002/adma.201504657>.
- Yang, H., Xiao, X., Li, Z., Li, K., Cheng, N., Li, S., Low, J.H., Jing, L., Fu, X., Achavananthadith, S., Low, F., Wang, Q., Yeh, P.L., Ren, H., Ho, J.S., Yeow, C.H., Chen, P.Y., 2020. Wireless Ti₃C₂T_xMXene Strain Sensor with Ultrahigh Sensitivity and Designated Working Windows for Soft Exoskeletons. *ACS Nano* 14, 11860–11875. <https://doi.org/10.1021/acsnano.0c04730>.
- Zamzami, M.A., Rabbani, G., Ahmad, A., Basalah, A.A., Al-Sabban, W.H., Ahn, S.N., Choudhry, H., 2022a. Fabrication and characterization of field effect transistor based on single walled carbon nanotubes. *J. King Saud Univ. - Sci.* 34, <https://doi.org/10.1016/j.jksus.2022.102137> 102137.
- Zamzami, M.A., Rabbani, G., Ahmad, A., Basalah, A.A., Al-Sabban, W.H., Nate Ahn, S., Choudhry, H., 2022b. Carbon nanotube field-effect transistor (CNT-FET)-based biosensor for rapid detection of SARS-CoV-2 (COVID-19) surface spike protein S1. *Bioelectrochemistry* 143, <https://doi.org/10.1016/j.bioelechem.2021.107982> 107982.
- Zhang, Z., Li, Y., Liang, C., Yu, G., Zhao, J., Luo, S., Huang, Y., Su, C., Xing, G., 2020a. In Situ Growth of MAPbBr₃ Nanocrystals on Few-Layer MXene Nanosheets with Efficient Energy Transfer. *Small* 16, 1. <https://doi.org/10.1002/sml.201905896>.
- Zhang, R., Rejeeth, C., Xu, W., Zhu, C., Liu, X., Wan, J., Jiang, M., Qian, K., 2019a. Label-Free Electrochemical Sensor for CD44 by Ligand-Protein Interaction. *Anal. Chem.* 91, 7078–7085. <https://doi.org/10.1021/acs.analchem.8b05966>.
- Zhang, Y.Z., Wang, Y., Jiang, Q., El-Demellawi, J.K., Kim, H., Alshareef, H.N., 2020b. MXene Printing and Patterned Coating for Device Applications. *Adv. Mater.* 32, 1–26. <https://doi.org/10.1002/adma.201908486>.
- Zhang, Y., Zalar, P., Kim, C., Collins, S., Bazan, G.C., Nguyen, T.Q., 2012. DNA interlayers enhance charge injection in organic field-effect transistors. *Adv. Mater.* 24, 4255–4260. <https://doi.org/10.1002/adma.201201248>.
- Zhao, J., Tang, Y., Cao, Y., Chen, T., Chen, X., Mao, X., Yin, Y., Chen, G., 2018. Amplified electrochemical detection of surface biomarker in breast cancer stem cell using self-assembled supramolecular nanocomposites. *Electrochim. Acta* 283, 1072–1078. <https://doi.org/10.1016/j.electacta.2018.07.002>.
- Zhu, W., Panda, S., Lu, C., Ma, Z., Khan, D., Dong, J., Sun, F., Xu, H., Zhang, Q., Zou, J., 2020. Using a Self-Assembled Two-Dimensional MXene-Based Catalyst (2D-Ni@Ti₃C₂) to Enhance Hydrogen Storage Properties of MgH₂. *ACS Appl. Mater. Interfaces* 12, 50333–50343. <https://doi.org/10.1021/acsaami.0c12767>.